Int J Adv Manuf Technol (2014) 72:729–738
DOI 10.1007/s00170-014-5705-y

ORIGINAL ARTICLE

Mathematic modeling and FE simulation of radial-axial ring rolling large L-section ring by shape axial roll

Pingzhen Zhou · Liwen Zhang · Sendong Gu · Jinhua Ruan · Lihong Teng

Received: 24 September 2013 / Accepted: 6 February 2014 / Published online: 25 February 2014

Abstract An accurate prediction of the ring diameter growth rate of a large L-section ring during radial-axial ring rolling (RARR) by a shape axial roll is quite essential because it determines the stability of the process and thus influences the quality of the rolled ring. In this paper, a mathematic model predicting the ring diameter of the large L-section ring during the new RARR process is first established. Then, 3D thermo-mechanical coupled rigid-plastic finite element (FE) models of the new RARR process are developed based on the implicit code DEFORM-3D to verify the mathematic model. By setting and adjusting the movements of the work rolls, large L-section rings are rolled. The effective strain distribution of the rolled ring is analyzed. Comparisons between the FE simulated and the mathematic predicted parameters including external diameter, growth rate of external diameter, and rotational speed of the rolling ring are made. The simulated and the predicted parameters are in good agreement, indicating that the mathematic model accurately predicted the size of the rolling ring and thus can be used to provide a guideline in real manufacturing of large L-section rings.

Keywords Large L-section ring · Shape axial roll · Radial-axial ring rolling · Diameter growth rate · FE

Nomenclature

V	Volume of the ring
D_0	External diameter of the billet
D	Instantaneous external diameter of the ring
D_1	Diameter of the drive roll
h_0	Initial height of the ring
h_s	Instantaneous height of the small ring
h_b	Instantaneous height of the big ring
d_0	Internal diameter of the billet
d_s	Instantaneous internal diameter of the small ring
d_b	Instantaneous internal diameter of the big ring
b_0	Initial thickness of the billet
b_1	Thickness of the big ring
n	Instantaneous rotational speed of the ring
n_D	Rotational speed of the drive roll
n_a	Rotational speed of the shape axial roll
L	Length of the work shape axial roll
θ	Cone angle of the axial roll
R_a	Working radius of the shape axial roll
v_w	Withdraw speed of the shape axial roll
v_D	Growth rate of the external diameter
v	Feed speed of the shape axial roll
t	Total rolling time

1 Introduction

Radial-axial ring rolling (RARR) is an advanced plastic deformation technique which reduces ring thickness, enlarges ring diameter, and forms ring cross section. As the advantages of load and energy saving, high material yield, small equipment tonnage, and little vibration, RARR has been increasingly employed to manufacture precise seamless annular rings with a variety of diameters, materials, and cross sections, which are widely used in all kinds of industries, such as machine, astronautics, railway, automobile, etc. [1]. Until now, researches on RARR have mainly been carried out by experiments [2–5] and theoretical methods [6–8]. Because of the advantages of revealing deformation law, illustrating

P. Zhou · L. Zhang (✉) · S. Gu · J. Ruan
School of Materials Science and Engineering, Dalian University of Technology, Dalian 116024, People's Republic of China
e-mail: commat@mail.dlut.edu.cn

L. Teng
Jianshe South Road No.32, Zunhua City 064200, Hebei Province, People's Republic of China

forming defect, and debunking microstructural evolution history, various attempts have been made to apply finite element (FE) methods to ring rolling [9–16]. However, most researches focus on large rectangular section rings or small profiled rings, as they are the basis.

An L-section ring is a typical profiled ring, which consists of a big rectangular section ring and a small rectangular section ring [17]. Traditionally, an L-section ring is rolled using a shape mandrel when the groove is in the inner layer or a shape drive roll when the groove is in the outer layer. Hua et al. [17, 18] studied the deformation behavior and biting condition of this ring rolling technique. In addition, Hua et al. [19] pointed out that the material flow between the big ring and the small ring is disadvantageous because it can lead to material accumulation at the step surface, which can hinder the step formation and ring enlargement. Moreover, the height of the groove is so low in some cases that it cannot be rolled using a shape mandrel or a shape drive roll.

Recently, a new RARR process in which a shape axial roll is used to form large a L-section ring has been proposed. In this method, as shown in Fig. 1, the shape axial roll both feeds downward and withdraws with the growth of the deformed ring. Because of the complexity of the deformation process, the match between the withdraw speed and the feed speed of the shape axial roll is extremely hard to promise. Li et al. [20] rolled a profiled heavy disk, and Hirt et al. [21] rolled a ring with a bulge on the axial end plane of the ring using a shape axial roll. In their experiments, the withdraw speed of the shape axial roll is controlled according to the measured rolling pressure or the measured diameter. However, the experiments are expensive and difficult to control. And, FE simulation is time consuming. Furthermore, the size parameters of L-section rings vary so that it is almost impossible to conduct FE simulations or experiments to investigate the ring diameter growth rate for every L-section ring. Therefore, an accurate prediction for the growth rate of the ring diameter is essential for this new technique.

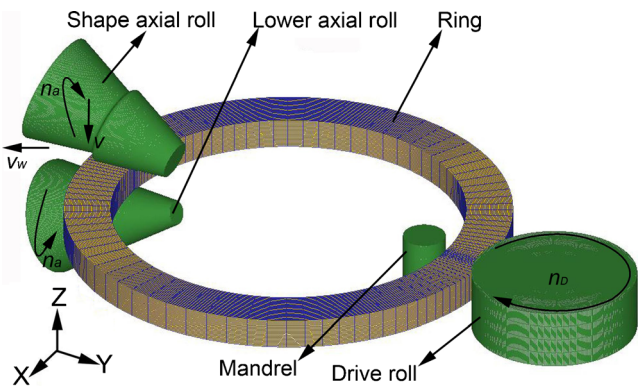

Fig. 1 Forming principle of the new RARR process

In this paper, the mathematic model, in which the slip between the shape axial roll and the ring, the penetration condition, and the biting condition are all taken into consideration, for predicting ring diameter during this new RARR process is proposed. Then, FE models are developed and verified. At last, the simulated ring diameters and rotational speeds are compared with the predicted ones. Also, the distribution of effective strain is analyzed.

2 Mathematic derivations of steady forming condition

2.1 Forming principle of the new RARR

RARR is an extremely complicated incremental, nonlinear, unstable plastic deformation process. Figure 1 shows the forming principle of RARR using a shape axial roll: the drive roll takes active rotation, and the mandrel takes passive rotation; the shape axial roll and the lower axial roll withdraw with the same speed and rotate along their axis with the same rotational speed but contrary directions; also, the shape axial roll feeds downward to form the profiled cross section of the ring.

During RARR, the ring is dually drawn into and rolled in the axial roll gap (formed by the lower axial roll and the shape axial roll) and the radial roll gap (formed by the mandrel and the drive roll). For a traditional RARR process, the ring rotates continuously because the drive roll rotates and the mandrel feeds toward the drive roll. In this new RARR process, the drive roll still rotates, but the mandrel does not feed toward the drive roll. However, the radial roll gap eliminates the spread produced by the axial roll gap, meaning that there is real feed amount for the mandrel. Therefore, the ring can be bitted into the roll gaps and can rotate continuously in this new RARR process.

The variation of the cross section before and after this new RARR process is shown in Fig. 2. The cross sections of the big ring and the small ring are both considered rectangular during the whole RARR process. In order to keep the RARR process steady, the shape axial roll should withdraw with the speed which is exactly equal to the growth rate of the external diameter of the deformed ring. Otherwise, the shape axial roll either prevents the ring from growing in the radial direction when the withdraw speed of the shape axial roll v_w is less than the growth rate of external diameter of the deformed ring v_D or pulls the deformed ring to make the ring an ellipse when v_w is greater than v_D.

2.2 Establish mathematic correlations of key variables

In order to minimize or even eliminate the dynamic collisions and vibrations between the deformed ring and the shape axial roll, it is essential to develop a proper mathematic model for the prediction of ring diameter.

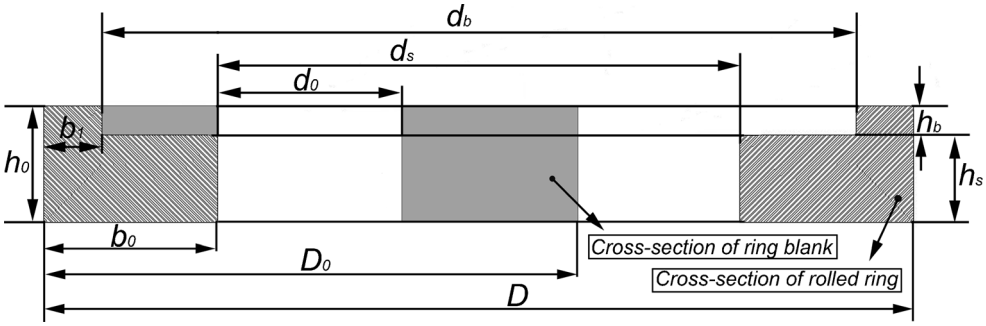

Fig. 2 Cross-section variation of the ring before and after RARR

2.2.1 Diameter of the deformed ring

For this new RARR process, the feed speed of the shape axial roll is relatively small and the mandrel does not feed toward the drive roll. Therefore, it is acceptable to assume that the deformed ring is comprised of two rectangular-section rings during the whole new RARR process. According to the volume constant principle during ideal plastic deformation, we have the following correlations:

$$V = \frac{\pi\left(D_0^2 - d_0^2\right)h_0}{4} \tag{1}$$

$$V = \frac{\pi\left(D^2 - d_s^2\right)h_s}{4} + \frac{\pi\left(D^2 - (D-2b_1)^2\right)h_b}{4} \tag{2}$$

Here, V represents the volume of the ring. D and d_s are the instantaneous external diameter and the instantaneous inner diameter of the small ring, respectively. The height of the big ring h_b is equal to the feed amount of the shape axial roll, and the total height of the ring h_0 keeps unchanged. Moreover, the thickness of both the big ring b_1 and the small ring which is equal to the thickness of the billet b_0 both keep constant.

$$h_b = \int_0^t v dt \tag{3}$$

$$h_s = h_0 - \int_0^t v dt \tag{4}$$

$$b_0 = \frac{D_0 - d_0}{2} = \frac{D - d_s}{2} \tag{5}$$

Substitute Eqs. (3), (4), and (5) into Eq. (2), and then substitute Eq. (2) into Eq. (1), the instantaneous external diameter of the deformed ring can be obtained.

$$D = \frac{\frac{V}{\pi} + h_0 b_0^2 - \left(b_0^2 - b_1^2\right)\int_0^t v dt}{h_0 b_0 + b_1 v t - b_0 \int_0^t v dt} \tag{6}$$

According to Eq. (6), it can be known that the instantaneous external diameter of the deformed ring can be known if the feed speed of the shape axial roll v is given. As v is a constant in this new RARR process, Eq. (6) can be rewritten as

$$D = \frac{\frac{V}{\pi} + h_0 b_0^2 - \left(b_0^2 - b_1^2\right)vt}{h_0 b_0 + b_1 v t - b_0 v t} \tag{7}$$

2.2.2 Movements of the shape axial roll

Figure 3 shows the relative position of the shape axial roll and the ring billet and its variation before and after the new RARR process. As shown in Fig. 3, the shape axial roll feeds downward, withdraws, and rotates with increasing ring diameter.

In order to guarantee the stability of the RARR process, the withdraw speed of the shape axial roll v_w should be the same with the growth rate of external diameter v_D. Therefore, the withdraw speed of the shape axial roll can be expressed as follows:

$$v_D = \frac{dD}{dt} \tag{8}$$

$$v_w = v_D \tag{9}$$

Substitute Eqs. (7) and (8) into Eq. (9), the withdraw speed of the shape axial roll, which is equal to the growth rate of external diameter of the deformed ring, can be expressed as follows.

$$v_w = \frac{v(b_1 - b_0)\left(h_0 b_0 b_1 - \frac{V}{\pi}\right)}{\left(h_0 b_0 + b_1 v t - b_0 v t\right)^2} \tag{10}$$

It can be known from Eq. (10) that the withdraw speed changes during the whole RARR process. In order to simplify the control system of the ring rolling mill, the withdraw speed of shape axial roll is fitted into a polygonal line, i.e., the withdraw speed is a constant during every time increment and differs for different time increments. Theoretically, the smaller the time increment ΔT is, the more accurate the

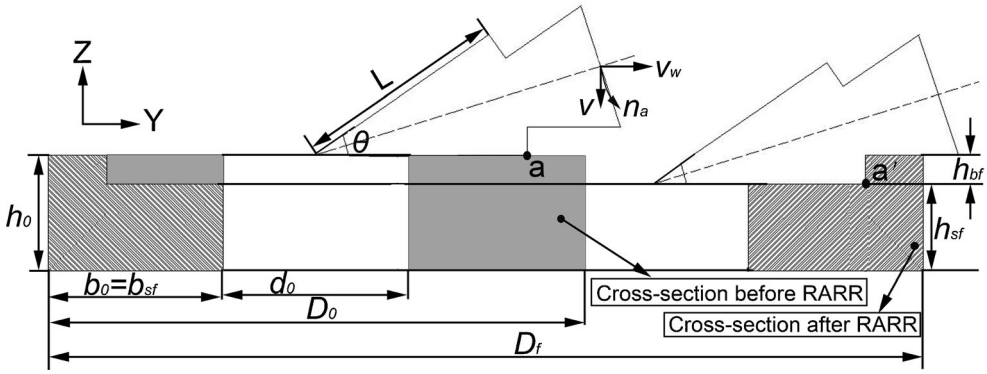

Fig. 3 Variation of shape axial roll before and after RARR

withdraw speed will be. The withdraw speed of the shape axial roll during every time increment can be expressed as follows:

$$v_w^{'} = \frac{\Delta D}{\Delta T} \tag{11}$$

Here, $v_w^{'}$ is the average withdraw speed of the shape axial roll during the time increment ΔT. Considering the ability of the control system, ΔT should be appropriately chosen during the real RARR process.

In order to obtain a relative minimum slip between the shape axial roll and the ring, the linear velocity of the shape axial roll at the contact points should be equal to or greater than that of the rotating ring. Generally, the linear velocities of the shape axial roll at the contact region are greater than that of the deformed ring when the linear velocity of the shape axial roll at the outermost layer of the ring is equal to or greater than the linear velocity of the ring at the outermost layer. That is, as illustrated in Fig. 3, at point a, the linear velocity of the shape axial roll should be equal to or greater than the linear velocity of the deformed ring during the whole RARR process. Assuming that there is no slide between the ring and the drive roll, the linear velocity of the outermost layer of the deformed ring is equal to the linear velocity of the drive roll. We have:

$$nD = n_D D_1 \tag{12}$$

As the diameter of the drive roll D_1 and the rotational speed of the drive roll n_D are given and the instantaneous external diameter of the deformed ring D can be known from Eq. (7), the rotational speed of the ring can be expressed as

$$n = \frac{n_D D_1 (h_0 b_0 + b_1 vt - b_0 vt)}{\frac{V}{\pi} + h_0 b_0^2 - (b_0^2 - b_1^2) vt} \tag{13}$$

In order to make sure that the linear velocity of the shape axial roll is equal to or greater than the linear velocity of the deformed ring at point a, the following equation should be satisfied:

$$n_a R_a \geq n\left(\frac{D}{2} - b_1\right) \tag{14}$$

Here, n_a is the rotational speed of the shape axial roll. R_a is the working radius of the shape axial roll at point a, and R_a can be expressed as follows:

$$R_a = L\sin\frac{\theta}{2} \tag{15}$$

Here, L is the length of the work shape axial roll, and θ is the angle of the shape axial roll. Substitute Eqs. (13) and (15) into Eq. (14), the rotational speed of the shape axial roll n_a can be written as follows:

$$n_a \geq \frac{n\left(\frac{D}{2} - b_1\right)}{L\sin\frac{\theta}{2}} \tag{16}$$

2.2.3 Reasonable range of the feed speed v

During this new RARR process, the ring should meet the penetration condition (the required minimum amount of height reduction per revolution) and the biting condition (the allowed maximum amount of height reduction per revolution) in the axial roll gap to make sure that the process can be accomplished successfully. According to Pan [22] and Zhou [23], we have

$$\Delta h_{a\min} \leq \Delta h_a \leq \Delta h_{a\max} \tag{17}$$

$$\Delta h_{a\min} = \frac{1.31 \times 10^{-2} h_0^2}{(L - b_0 + b_1)\tan\frac{\theta}{2}} \tag{18}$$

$$\Delta h_{a\max} = 4\beta^2 L\tan\frac{\theta}{2} \tag{19}$$

where β is the friction angle (the half of the contact angle between the axial roll and the ring) in the axial roll gap, and Δha is the axial feed amount of the shape axial roll per revolution. $\Delta h_{a\min}$ and $\Delta h_{a\max}$ are the permitted minimum and maximum feed amounts per revolution of the axial roll gap, respectively. Assuming that there is no slide between the ring and the drive roll, Δh_a can be described as

$$\Delta h_a = \frac{\pi D v}{n_D D_1} \tag{20}$$

Substitute Eqs. (18), (19), and (20) into Eq. (17), the range of the feed speed of the shape axial roll can be deduced.

$$\frac{1.31\times 10^{-2} n_D D_1 h_0^2}{\pi D(L-b_0+b_1)\tan\frac{\theta}{2}} \le v \le \frac{4 n_D D_1 \beta^2 L\tan\frac{\theta}{2}}{\pi D} \tag{21}$$

During the new RARR process, the axial rolling force and vibration augment with increasing feed speed [1]. Therefore, the feed speed of the shape axial should be as small as possible on the premise that the penetration condition is met.

3 3D coupled thermo-mechanical FE model

3.1 Developing FE model

In order to verify the mathematic model, 3D thermo-mechanical coupled rigid-plastic FE models are developed on the platform of general-purpose commercial FE software of DEFORM. The simulation parameters are summarized in Table 1, and the size parameters of the billet and the rolled ring are presented in Table 2. Actual sized FE models, as shown in Fig. 1, are developed to verify the reliability of the mathematic model. Both the size of the ring and the feed speed of the shape axial roll are changed to further validate the mathematic model.

Table 1 The common simulation parameters

Parameter	Value
Diameter of the drive roll, D_1 (mm)	1,100
Diameter of the mandrel, D_2 (mm)	280
Cone angle of the axial roll, θ (°)	35
Rotational speed of drive roll, n_D (rad/s)	2.2
Temperature of the billet, (°C)	1,200
Temperature of the environment, (°C)	20
Temperature of the rolls, (°C)	150
Feed speed of the shape axial roll, v (mm/s)	0.2/0.3

Table 2 The different simulation parameters

Parameter	Geometry A	Geometry B
External diameter of the billet, D_0 (mm)	2,985	2,385
Inner diameter of the billet, d_0 (mm)	2,368	1,768
Thickness of the billet, b_0 (mm)	308.5	308.5
External diameter of the ring, D_f (mm)	3,574	2,838
Inner diameter of the small ring, d_{sf} (mm)	2,957	2,221
Inner diameter of the big ring, d_{bf} (mm)	3,414	2,678
Height of the big ring, h_{bf} (mm)	50	50
Height of the small ring, h_{sf} (mm)	150.5	150.5

The main features of the FE models are described as follows:

1. A Ring-Rolling solver in DEFORM-3D, which increases the mesh density in the roll gap region and decreases the mesh density in other regions during the FE simulation process, is adopted to improve the simulation accuracy and efficiency.
2. The coupled thermo-mechanical brick element with eight nodes is adopted to discretize the ring. The fully automatic Arbitrary Lagrangian and Euler adaptive remeshing technique is employed to guarantee a high-quality mesh during the whole FE simulation process.
3. Four contact pairs are defined between the ring and the rolls, and the friction coefficient is set as 0.35 [23–25]. Compared with the ring, the variations of deformation and temperature of the rolls are so small that the rolls are treated as analytically rigid and isothermal bodies. There is internal heat generation caused by plastic work and

Table 3 Parameters of radial-axial ring rolling model

Parameters	Values
External diameter of the billet (mm)	1,252
Internal diameter of the billet (mm)	952
Height of the billet (mm)	230
External diameter of the rolled ring (mm)	2,000
Internal diameter of the rolled ring (mm)	1,800
Height of the rolled ring (mm)	200
Radius of main roll (mm)	450
Radius of idle roll (mm)	150
Angle of conical roll (°)	35
Friction coefficient	0.35
Feed rate of idle roll (mm/s)	1.5
Feed rate of conical roll (mm/s)	1

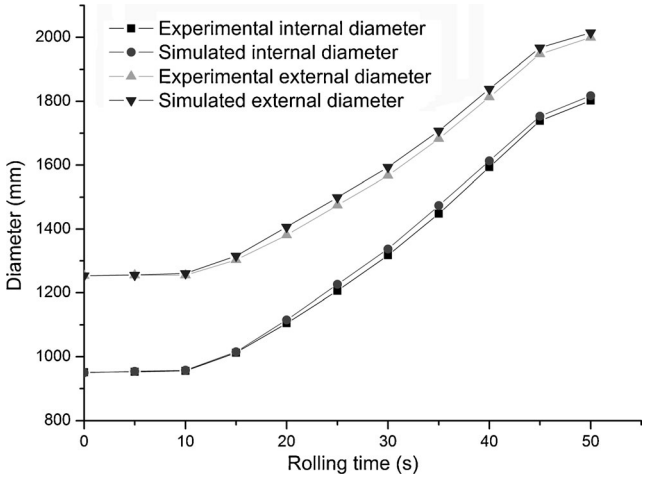

Fig. 4 Comparisons of diameters between simulation and experiment

friction and heat transfer at the contact surfaces of the ring. Moreover, there are heat convection and thermal radiation from all the surfaces of the ring.

4. The ring material is 42CrMo alloy steel. Its variation of heat capacity within the rolling temperature range, 800 to 1,400 °C, is taken into consideration. The coefficients of heat convection, heat radiation, and heat transmission are 0.02, 0.7, and 10 N/s/mm/K, respectively.

   The material's flow stress is determined by temperature, strain rate, and strain. During the FE analysis, the variation of flow stress under a temperature range of 800 to 1,400 °C, a strain rate range of 1.6 to 40, and a strain range of 0 to 1 is considered. The conversation rate of plastic work to heat is assumed as 0.9.
5. The axial height of the big ring augments while that of the small ring reduces as the shape axial roll feeds downward. Moreover, the shape axial roll withdraws with a speed which is equal to the growth rate of the external diameter.

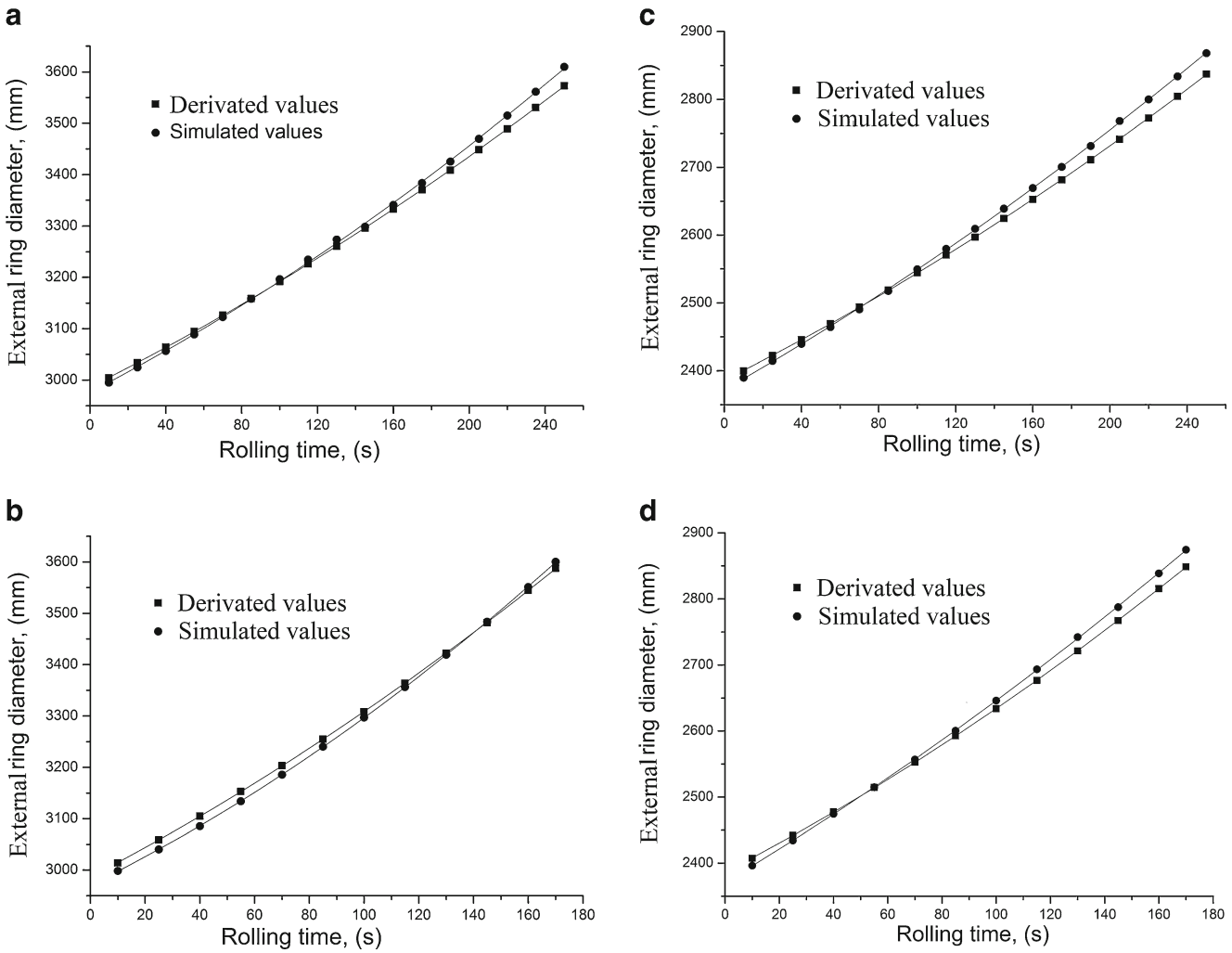

Fig. 5 Comparisons of the simulated and the predicted external diameters: **a** Geometry A, v=0.2 mm/s; **b** Geometry A, v=0.3 mm/s; **c** Geometry B, v=0.2 mm/s; **d** Geometry B, v=0.3 mm/s

Therefore, the radial thickness of the big ring keeps constant. After the external diameter reaches the desired value, the shape axial roll stops feeding and the ring rolling process stops.

3.2 Verification of FE model

In order to validate the prediction capability of the developed FE models, an FE model, which corresponds to the ring rolling experiment of Xu [25], is developed on the same platform, and comparisons between the simulated ring diameters and the measured ones are made. The process parameters are summarized in Table 3.

As presented in Fig. 4, the FE simulated internal and external diameters show good agreement with the experimental ones, meaning that the FE model developed to verify the mathematic model can also be considered reliable.

4 Results and discussion

4.1 Growth rate of the external diameter

Figure 5 shows the comparisons of the predicted and the simulated external diameters of the deformed ring under different conditions. It can be seen from Fig. 5 that the predicted external diameters grow smoothly and regularly and that the simulated external diameter matches well with the predicted results with the progress of RARR in all conditions. In addition, Fig. 5 shows that the simulated external diameters of the rolled rings are slightly greater than the predicted ones after the rings are rolled. This is because the cross sections of the rolled rings are not ideal during the RARR process, leading the growth rates of the external diameters to increase faster than the predicted ones.

It can be seen from Fig. 5a, b that the external diameters of geometry A have increased more than 600 mm after the shape

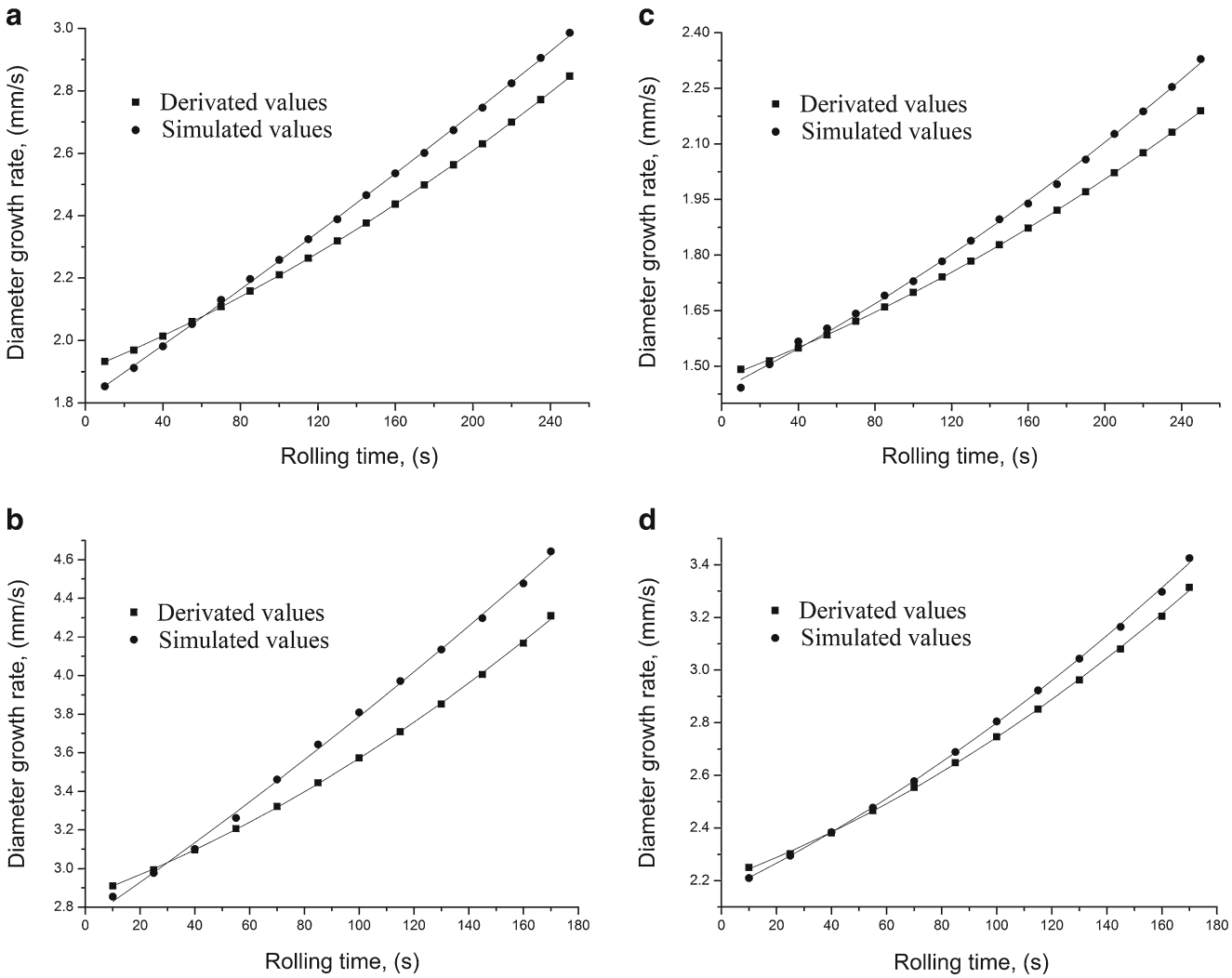

Fig. 6 Comparisons of the simulated and the predicted growth rates of external diameter: **a** Geometry A, v=0.2 mm/s; **b** Geometry A, v=0.3 mm/s; **c** Geometry B, v=0.2 mm/s; **d** Geometry B, v=0.3 mm/s

axial roll has fed 50 mm. And, as presented in Fig. 5c, d, the external diameters of geometry B have increased less than 500 mm after the shape axial roll has fed 50 mm. Comparing Fig. 5a, b with Fig. 5c, d, it can be known that the increasing amount of external diameter increases with augmenting billet diameter.

Figure 6 provides the comparisons of the predicted and the simulated growth rates of the external diameter of the ring for different feed speeds of the shape axial roll v and different sizes of the billets. It can be known from Fig. 6 that the simulated growth rates are slightly slower than the predicted ones at first and then become slightly faster than the predicted ones. In general, the simulated growth rates of external diameter under all conditions match well with the corresponding mathematic prediction.

Comparing Fig. 6a with b or c with d, it can be inferred that the diameter growth rate climbs with increasing feed speed of the shape axial roll. Furthermore, it can be known from Fig. 6 that the diameter growth rate decreases with decreasing billet diameter.

4.2 Rotation of the deformed ring

Figure 7 compares the simulated and the predicted rotational speeds of the deformed ring under different conditions. It can be seen from Fig. 7 that the predicted rotational speeds of the deformed ring decrease almost linearly with the progress of RARR in all conditions. It also can be known from Fig. 7 that the simulated rotational speeds of the deformed ring first exceed the predicted ones slightly and become less than the predicted ones later. Combining with Fig. 6, it can be known that the simulated external diameters are first smaller than the predicted ones and become larger than the predicted ones later. As the linear velocities of the outmost layer of the deformed rings are constant, the simulated rotational speeds are slightly greater than the predicted ones at first and become smaller

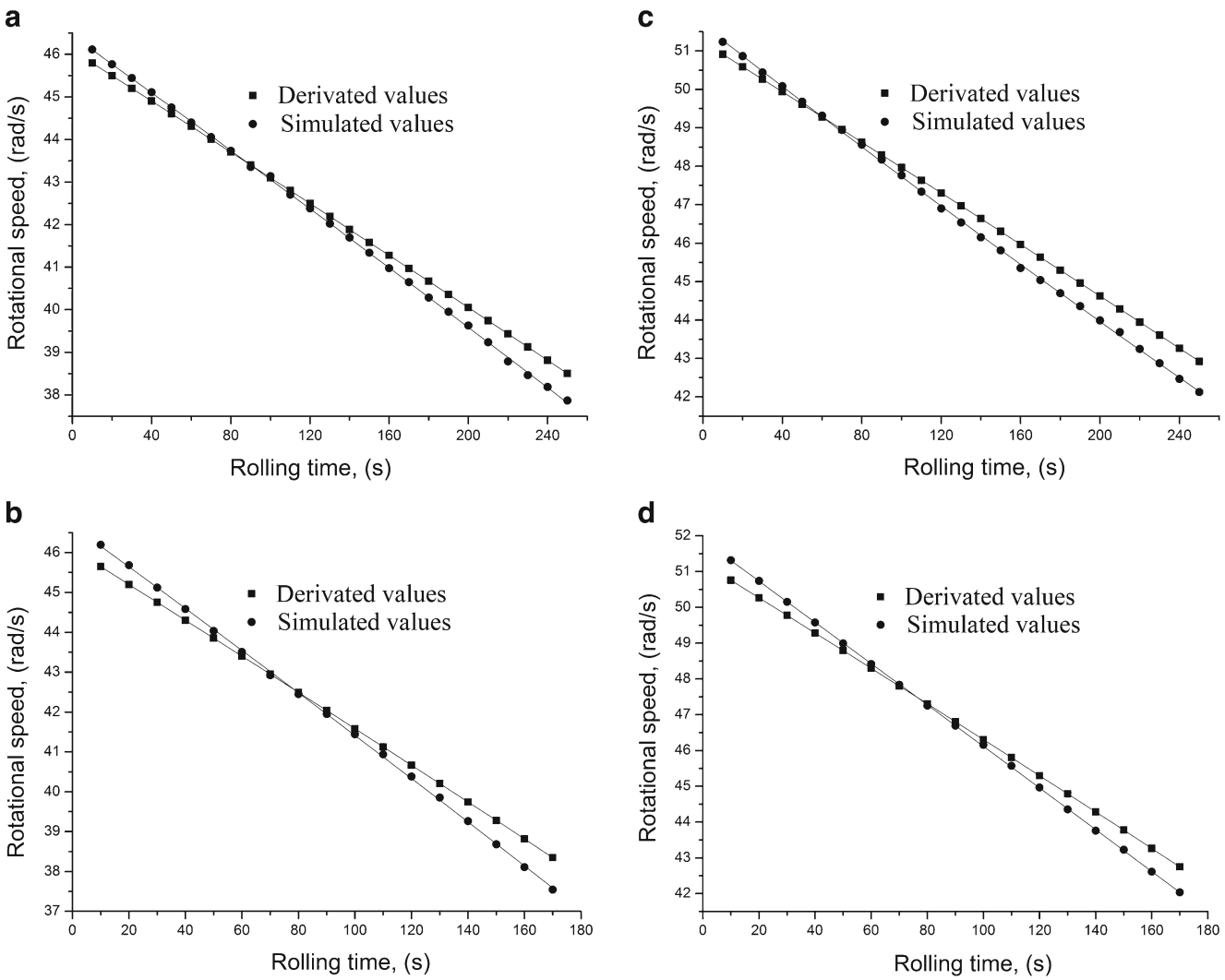

Fig. 7 Rotational speeds under different conditions: **a** Geometry A, v=0.2 mm/s; **b** Geometry A, v=0.3 mm/s; **c** Geometry B, v=0.2 mm/s; **d** Geometry B, v=0.3 mm/s

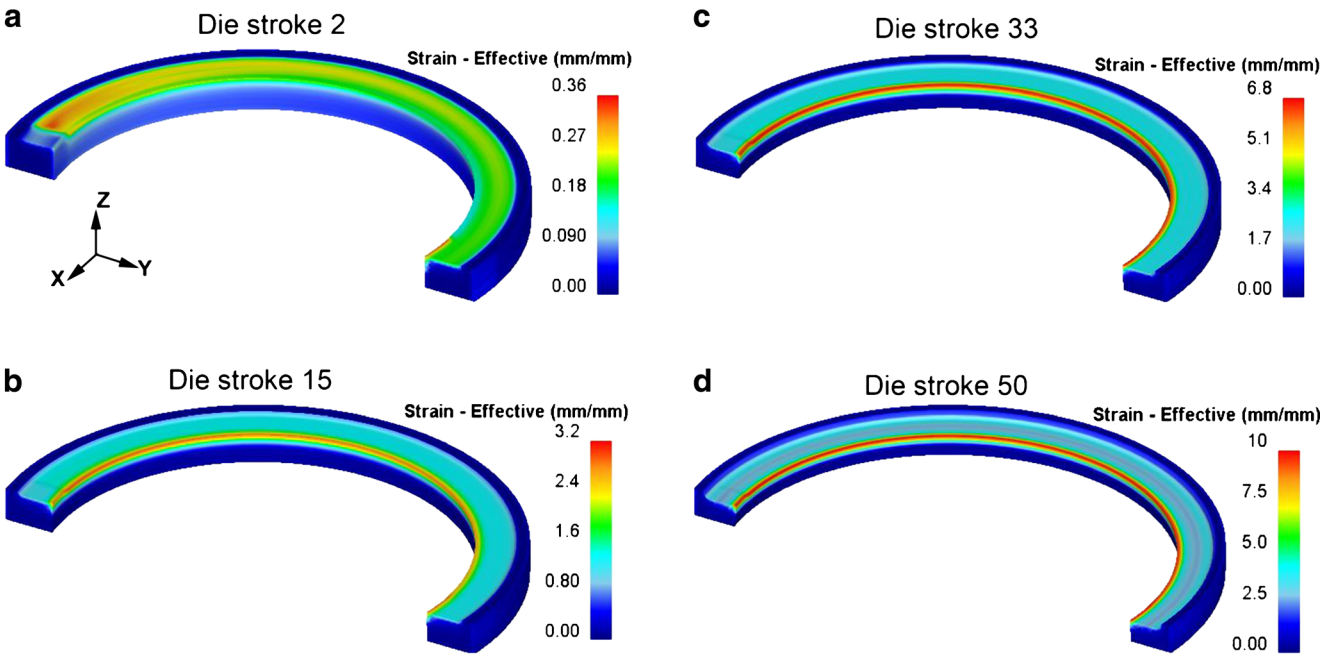

Fig. 8 Configurations and contours of effective strain at different feed amounts of shape axial roll (Geometry A, v=0.3 mm/s)

than the predicted ones at last. Generally, the simulated results match well with the predicted ones under different conditions.

Comparing Fig. 7a with b or c with d, it can be known that the initial and the final rotational speeds of the ring are the same for the same billet. However, the total rolling time decreases significantly with increasing feed speed of shape axial roll, leading the average rotational speeds to decrease sharply with increasing feed speed of the shape axial roll. Comparing Fig. 7a with c or b with d, it can be known that the rotational speeds increase with decreasing diameter of ring billet.

4.3 Distribution of effective strain

Figure 8 shows the configurations of the deformed ring and the contour of effective strain at different feed amounts of the shape axial roll. It can be known from Fig. 8 that the distribution of the effective strain is inhomogeneous in the hoop direction at first and gets homogeneous after several rotations, which indicates that the ring is drawn into the roll gaps continuously and rotates smoothly in this model. Furthermore, the effective strain mainly focuses on the end plane of the small ring as it is compressed by the axial roll gap continuously. The spread is produced and eliminated repeatedly by the radial roll gap and the axial roll gap in the inner layer of the small ring, so that the biggest effective strain occurs here.

5 Conclusion

A mathematic model of a new RARR process for a large L-section ring, in which the variation of the cross section, the steady forming condition, and the penetration and biting conditions are all taken into consideration, for the prediction of ring diameter has been established. In order to validate this mathematic model, 3D thermo-mechanical coupled rigid-plastic FE models are developed on the platform of DEFORM-3D. The simulation results show that deformation mainly occurs at the small ring and that the distribution of strain is homogeneous in the hoop direction in this new RARR process. Furthermore, both the FE simulated growth rate of the ring diameter and the rotational speed of the deformed ring match well with the mathematic predicted results, meaning that the mathematic model can accurately predict the size parameters of the rolling ring.

Acknowledgement The authors would like to appreciate the financial support from Tangshan Zhiwei Ltd. Co. for this research.

Conflict of interest The authors declare that they have no conflict of interest.

Reference

1. Hua L, Huang XG, Zhu CD (2001) Theory and technology of ring rolling. China Mechanical Industry, Beijing, In Chinese
2. Johnson W, MacLeod I, Needham G (1968) An experimental investigation into the process of ring or metal tyre rolling. Int J Mech Sci 10:455–68
3. Hawkyard JB, Johnson W, Kirkland J, Appleton E (1973) Analysis for roll force and torque in ring rolling with some supporting experiments. Int J Mech Sci 15:873–93
4. Mamalis AG, Hawkyard JB, Johnson W (1976) Spread and flow patterns in ring rolling. Int J Mech Sci 18:11–16

5. Mamalis AG, Johnson W, Hawkyard JB (1976) On the pressure distribution between stock and rolls in ring rolling. P I Mech Eng C-J Mec 18:184–196
6. Mamalis AG, Johnson W, Hawkyard JB (1976) Pressure distribution, roll force and torque in cold ring rolling. P I Mech Eng C-J Mec 18: 197–209
7. Hua L, Zhao ZZ (1997) The extremum parameters in ring rolling. J Mater Process Technol 69:273–276
8. Lugora CF, Bramley AN (1987) Analysis of spread in ring rolling. Int J Mech Sci 29(2):149–157
9. Utsunomiya H, Saito Y, Shinoda T, Takasu I (2002) Elastic–plastic finite element analysis of cold ring rolling process. J Mater Process Technol 125&126(9):613–618
10. Xie CL, Dong XH, Li SJ, Huang SH (2000) Rigid-viscoplastic dynamic explicit FEA of the ring rolling process. Int J Mach Tool Manuf 40(1):81–93
11. Davey K, Ward MJ (2002) A practical method for finite element ring rolling simulation using the ALE flow formulation. Int J Mech Sci 44: 165–190
12. Yang H, Guo LG, Zhan M (2006) Research on the influence of material properties on cold ring rolling processes by 3D-FE numerical simulation. J Mater Process Technol 177:634–638
13. Tian L, Luo Y, Mao HJ, Hua L (2013) A hybrid of theory and numerical simulation research for virtual rolling of double-groove ball rings. Int J Adv Manuf Technol 69:1–13
14. Li LY, Li X, Liu J, He Z (2013) Modeling and simulation of cold rolling process for double groove ball-section ring. Int J Adv Manuf Technol 69:1717–1729
15. Zhou J, Wang FL, Wang MH, Xu WJ (2013) Study on forming defects in the rolling process of large aluminum alloy ring via adaptive controlled simulation. Int J Adv Manuf Technol 55:95–106
16. Wang M, Yang H, Zhang C, Guo LG (2013) Microstructure evolution modeling of titanium alloy large ring in hot ring rolling. Int J Adv Manuf Technol 66:1427–1437
17. Hua L, Qian DS, Pan LB (2009) Deformation behaviors and conditions in L-section profile cold ring roll. J Mater Process Technol 209: 5087–5096
18. Qian DS, Hua L, Pan LB (2009) Research on gripping conditions in profile ring of raceway groove. J Mater Process Technol 209: 2794–2802
19. Qian DS, Hua L (2010) Blank design optimization for stepped-section profile ring rolling. Sci China Technol Sc 53(6):1612–1619
20. Li QH, Wu LB, Li FG, Liu TY, Wang SG, Wei ZJ, Su CM (2013) Experiments study on the rolling process for heavy disk. Int J Adv Manuf Technol 65:1171–1175
21. Jenkouk V, Hirt G, Seitz J (2013) Numerical simulations supporting the process design of ring rolling processes. The 11th International Conference on Numerical Methods in Industrial Forming Processes, AIP Conf. Proc 1532:695–700
22. Pan LB (2007) On deformation laws and CAPP system for radial-axial ring rolling. Dissertation, Wuhan University of Technology (in Chinese)
23. Zhou G, Hua L, Qian DS (2011) 3D coupled thermo-mechanical FE analysis of roll size effects on the radial-axial axial ring rolling process. Comp Mater Sci 50:911–924
24. Zhou G, Hua L, Qian DS, Shi DF, Li HX (2012) Effects of axial rolls motions on radial-axial rolling process for large-scale alloy steel ring with 3D coupled thermo-mechanical FEA. Int J Mech Sci 59:1–7
25. Xu WJ, Yang XB, Gong XT, Zhou J (2012) A new mathematical model for predicting the diameter expansion of flat ring in radial-axial ring rolling. Int J Adv Manuf Technol 60:913–921